# Implicit gradient reconstruction (IGR) method for compressible flow simulation

**Manish K Singh[1,2], N Munikrishna[3], V Ramesh[1], N Balakrishnan[4*]**

[1] Scientist, Council of Scientific and Industrial Research-National Aerospace Laboratories, Bangalore, India
[2] Research scholar, Indian Institute of Science, Bangalore, India
[3] Chief Technology Officer, S & I Engineering Solution Pvt. Ltd. Bangalore, India
[4] Associate Professor, Indian Institute of Science, Bangalore, India

*Email: nbalak@aero.iisc.ernet.in

**Abstract.** The classical CIR scheme is modified by introducing a $\phi$ parameter which allows an explicit control of dissipation. Also, this permits a seamless integration of the upwind and central difference based schemes. It is demonstrated that the $\phi$ parameter can be linked to solution reconstruction and thus second order accuracy can be achieved effectively with a first order formula. An objective way of determining $\phi$ based on solution gradients on the volume interface is established. These gradients in turn are also used for viscous flux computation and therefore come at no additional cost. The efficacy of the proposed methodology is established by solving a number of standard test problems, both in 1D and 2D.

## 1. Introduction

One of the important developments in the area of upwind schemes is the development of Modified CIR (MCIR) schemes [1]. It simply involves introducing an additional $\phi$ parameter in the classical CIR scheme, which allows an explicit control of the resulting dissipation. This methodology has been successfully used in conjunction with the framework provided by the kinetic theory of gases for solving many problems of relevance to aerospace industry [2, 3]. The present effort is to further extend the scope of this methodology, by introducing a family of $\phi$ schemes, which provides a seamless framework for integrating upwind and central difference type schemes. It is demonstrated that the $\phi$ parameter can be linked to the solution gradients resulting from a reconstruction procedure and therefore the use of appropriate $\phi$ can be considered as an implicit way to do solution reconstruction. In this work, care is taken to ensure the effort needed for gradient finding for determination of $\phi$ is no more than what is needed for viscous flux computation. The resulting procedure, which can be used in conjunction with either flux vector splitting or flux difference splitting schemes, is simple, efficient and obviates the need to store solution gradients, leaving significantly less memory foot print as compared to classical linear reconstruction procedure.

## 2. Methodology

Consider the linear convection equation,

$$u_t + cu_x = 0 \tag{1}$$

where, the property $u$ gets convected with a speed $c$. The MCIR implementation reads (Figure 1),

$$\frac{u_j^{n+1}}{\Delta t} + \frac{c+\phi|c|}{2}\frac{u_j^n - u_{j-1}^n}{\Delta x} + \frac{c-\phi|c|}{2}\frac{u_{j+1}^n - u_j^n}{\Delta x} = 0 \tag{2}$$

where, $\phi$ is a user defined parameter. Referring to the Figure 2, representing the convection of a linear profile over a time step $\Delta t$, the time averaged flux on the volume interface $j + \frac{1}{2}$ is given by,

$$< f_{j+\frac{1}{2}} > = c\left(u_j^n - \frac{(1-\lambda)}{2}\delta u_j^n\right) = cu_j^n + \frac{1}{2}(c - \phi|c|)\delta_+ u_j^n \quad (3)$$

where, the Courant number $\lambda = \frac{|c|\Delta t}{\Delta x}$ and $\delta u_j^n$ is an undivided difference representing the solution gradient in volume *j* and $\delta_+ u_j = u_{j+1} - u_j$ . For an MCIR scheme, it is easy to show that,

$$\left(\delta u_j^n\right)_{MCIR} = \frac{(1-\phi)}{1-\lambda}\delta_+ u_j^n \quad (4)$$

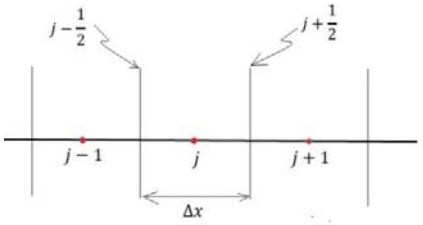


**Figure 1.** One dimensional stencil

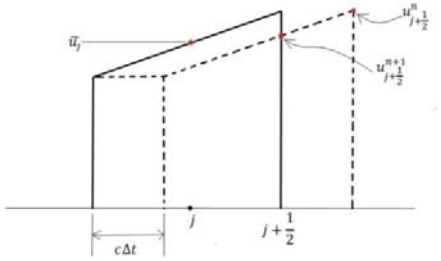


**Figure 2.** Reconstruction procedure

It is noteworthy to observe that for $\phi = \lambda$, the MCIR gradient reduces to the gradient corresponding to the Lax Wendroff scheme, i.e., $\left(\delta u_j^n\right)_{MCIR} = \delta_+ u_j^n = \left(\delta u_j^n\right)_{LW}$. This observation is very interesting in the sense that a family of $\phi$ schemes represented by CIR scheme for $\phi$ = 1.0 on one end and a spatially centered scheme for $\phi$ = 0.0 on the other end, with varying gradient representation within the finite volume, can be presented in the framework provided by MCIR. It is important to note that this gradient representation is rather implicit as against the classical formulations, where the gradients are computed explicitly in the reconstruction step and therefore the resulting procedure is referred to as Implicit Gradient Reconstruction (IGR) method. At this stage, it is worth remarking that negative values of $\phi$ would result in an unstable semi-discrete equation and $\phi$ > 1.0 will accentuate loss in monotonicity. Therefore $\phi$ is bounded between 0.0 and 1.0. The inference presented above also provides a means to objectively fix the value of $\phi$. This is achieved by equating the interfacial flux as obtained using a classical reconstruction scheme and the MCIR scheme:

$$f_{j+\frac{1}{2}} = \frac{c+|c|}{2}\left(u_j + \frac{\delta u_j}{2}\right) + \frac{c-|c|}{2}\left(u_{j+1} - \frac{\delta u_{j+1}}{2}\right) = \frac{c+\phi_{\frac{1}{2}}|c|}{2}u_j + \frac{c-\phi_{\frac{1}{2}}|c|}{2}u_{j+1} \quad (5)$$

This results in the following expression for $\phi$ associated with the interface $j + \frac{1}{2}$:

$$\phi_{\frac{1}{2}} = 1 - \frac{1}{2}\left(1 + \frac{c}{|c|}\right)\frac{\delta u_j}{\delta_+ u_j} - \frac{1}{2}\left(1 - \frac{c}{|c|}\right)\frac{\delta u_{j+1}}{\delta_+ u_j} \quad (6)$$

It is interesting to note that IGR method chooses the gradient from the upwind cell in the computation of $\phi$. The above expression also suggests that if the gradients used in the computation of $\phi$ are monotonicity preserving then the resulting MCIR scheme will also be monotonicity preserving. However, at this stage it appears as though the projected advantage of IGR method in not requiring an explicit gradient computation is not satisfied as gradients are required even for the determination of $\phi$. The above paradox is resolved by imposing an additional constraint that gradient finding associated with the IGR procedure should be limited to that needed for viscous flux computation. This is better explained in the case of 2D, presented in Figure 3, which depicts the determination of $\phi$ on the K[th] interface between cells *j* and *k*. The expression for $\phi_K$ in 2D reduces to

$$\phi_K = 1 - \frac{1}{2}\left(1 + \frac{\vec{C}.\hat{n}_k}{|\vec{C}.\hat{n}_k|}\right)\frac{\delta u_{Kj}}{\delta_+ u_K} - \frac{1}{2}\left(1 - \frac{\vec{C}.\hat{n}_k}{|\vec{C}.\hat{n}_k|}\right)\frac{\delta u_{Kk}}{\delta_+ u_K} \qquad \text{with} \quad \delta_+ u_K = u_k - u_j, \quad \overrightarrow{r_{kj}} = \vec{r}_k - \vec{r}_j$$

$$\delta u_{Kj} = \left(\nabla u_{Kj}.\hat{n}_k\right)\left|\overrightarrow{r_{kj}}\right|, \qquad \delta u_{kk} = \left(\nabla u_{Kk}.\hat{n}_k\right)\left|\overrightarrow{r_{kj}}\right|$$

where, $\nabla u_{Kj}$ and $\nabla u_{Kk}$ are gradients computed on the left and right lobes of the covolume constructed around the K[th] interface using Green-Gross procedure. $\hat{n}_k$ is the unit vector normal to the K[th] interface.

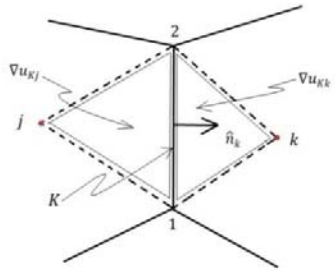


**Figure 3.** IGR procedure in 2D

It is evident from the above formula; computed gradients for determination of $\phi$ are essentially as needed for viscous flux computations. Also, all operations associated with the computation of $\phi$ are limited to the data associated with the corresponding face, which allows us to integrate the determination of $\phi$ with the face based procedure needed for the computation of both inviscid and viscous fluxes. Extension of the above procedure to Euler equations is rather straight forward, with its application to individual characteristic variables and the associated wave speeds. This would amount to recovering the gradients associated with the characteristic variables *W* from the gradients of the primitive variables using the following expressions for 1D and 2D, respectively:

$$(DW)_{1D} = \begin{bmatrix} \frac{dp-\rho c du}{2c^2} \\ -\frac{dp-c^2 d\rho}{2c^2} \\ \frac{dp+\rho c du}{2c^2} \end{bmatrix}, \qquad (DW)_{2D} = \begin{bmatrix} \frac{dp-\rho c dq_n}{2c^2} \\ -\frac{dp-c^2 d\rho}{2c^2} \\ \frac{dp+\rho c dq_n}{2c^2} \\ \rho dq_l \end{bmatrix} \quad \text{and} \quad \begin{aligned} q_n &= u.n_x + v.n_y \\ q_l &= -u.n_y + v.n_x \end{aligned}$$

where, $\rho$, *u*, *v* and *p* are density, velocity component in x-direction, velocity component in y-direction and pressure, respectively. Once the $\phi$ values associated with the individual characteristic variables are known, any flux formula like the one by Steger and Warming [4] or by Roe [5], can be easily modified to include the $\phi$ parameter associated with IGR. The IGR Roe flux formula (a modified Roe flux formula), in 2D is presented below:

$$\left(F_{IGR\_Roe}\right)_I = \frac{F_{\perp L}+F_{\perp R}}{2} - \frac{1}{2}\sum_i\left(\alpha_i\ \phi_i\ |\lambda_i|\ \vec{r}_i\right) \tag{7}$$

where, $F_{\perp L}/F_{\perp R}$ denotes the Euler flux normal to the interface. $\alpha_i$ and $\lambda_i$ denotes strength and eigenvalue of *i*[th] wave, respectively, computed from Roe averaged matrix. $\vec{r}_i$ is Eigenvector corresponding to *i*[th] wave.

For IGR Steger and Warming (IGR_SW) flux formula, positive and negative part of the eigenvalues are computed as $\lambda_i^{\pm} = \frac{\lambda_i \pm \phi_i|\lambda_i|}{2}$, and first order Steger and Warming flux formula is used with these eigenvalues. The eigenvalues are defined as $\lambda_1 = u.n_x + v.n_y = v_n$ , $\lambda_2 = v_n + c$ , $\lambda_3 = v_n - c$ then IGR_SW flux formula is given by

$$\left(F_{IGR\_SW}\right)^{\pm} = \frac{\rho}{2\gamma}\begin{pmatrix} \alpha \\ \alpha u + c\left(\lambda_2^{\pm} - \lambda_3^{\pm}\right)n_x \\ \alpha v + c\left(\lambda_2^{\pm} - \lambda_3^{\pm}\right)n_y \\ \alpha\frac{u^2+v^2}{2} + cv_n\left(\lambda_2^{\pm} - \lambda_3^{\pm}\right) + c^2\frac{\lambda_2^{\pm}+\lambda_3^{\pm}}{\gamma-1} \end{pmatrix} \quad \text{where} \quad \alpha = 2(\gamma-1)\lambda_1^{\pm} + \lambda_2^{\pm} + \lambda_3^{\pm}$$

## 3. Results

### *3.1 1D test case*

The Standard test case of shock tube problem is selected to test the IGR methodology [6]. The diaphragm is located at $x_0$=0.5 with initial left and right conditions given in table 1. A total of 100 points are used for flow simulation. The Exact solution at time t=0.2 is compared with Roe 2nd order, Steger and Warming (SW) 2nd order, SW 1st order and IGR scheme which modified 1st order SW flux formulation. The density, velocity, pressure and internal energy comparisons are given in Figures 4(a), 4(b), 5(a) and 5(b), respectively. It is evident that IGR scheme improves 1st order SW solution significantly and are comparable to the 2nd order Roe and SW schemes.

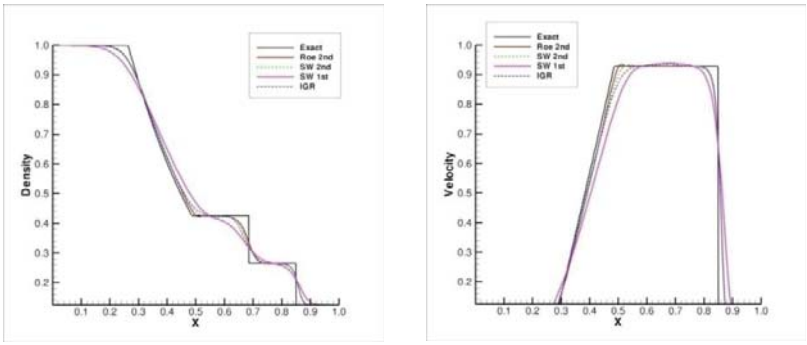


(a) (b)

**Figure 4.** Shock Tube problem (a) Density plot (b) Velocity plot

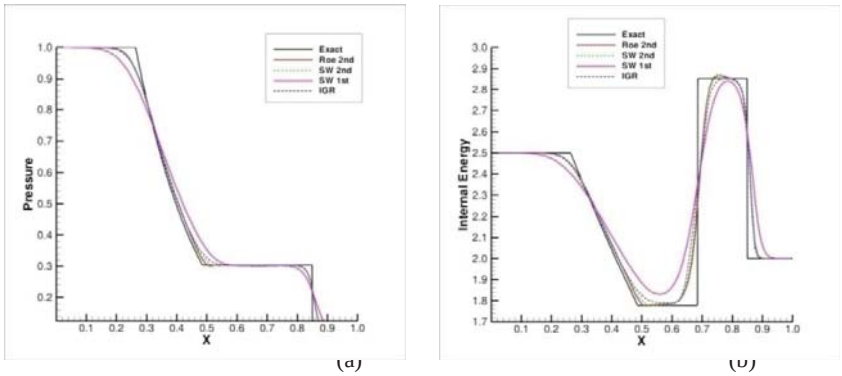


(a) (b)

**Figure 5.** Shock Tube problem (a) Pressure plot (b) Internal energy plot

**Table 1.** Shock tube initial condition

| Parameter | Left State | Right state |
|---|---|---|
| $\rho$ | 1.0 | 0.125 |
| $u$ | 0.0 | 0.0 |
| $p$ | 1.0 | 0.1 |

### *3.2 2D Test cases*

The IGR methodology have been implemented in HiFUN 2D solver using Roe and SW flux formulation and called as IGR_Roe and IGR_SW, respectively. HiFUN 2D is a finite volume based solver which has been extensively validated for variety of test cases (http://www.cfdcenter.aero.iisc.ernet.in). To demonstrate the capability of IGR methodology, we have selected 3 test cases for flow over NACA 0012 airfoil. The

computations from IGR_Roe and IGR_SW are compared with conventional 2nd order Roe and SW schemes which use conventional gradient reconstruction to achieve 2nd order of spatial accuracy. An unstructured grid with 6950 triangular cells is used for all these computations.

*3.2.1 Case 1:* The first 2-D test case selected is inviscid flow computation over NACA 0012 airfoil at M=0.63 and α=2°. This is a standard test case which has been used in GAMM workshop [7]. The pressure coefficient (Cp) comparison is depicted in Figure 6(a). It is observed that IGR_Roe computation is matching very well with those from 2nd order Roe and SW. The Euler computations from IGR_SW is close to the 2nd order Roe and SW at all the locations except at the suction peak where it's slightly under-predicting it. The density residue ($\log_{10}$) plot is given in Figure 6(b). It is evident that IGR_Roe and Roe 2nd order residue pattern are very close to each other. The Cp contour plots are matching quite well with each other [Figures 7(a)-7(d)]. The comparison between lift coefficient (CL) and drag coefficient (CD) are given in table 2.

**Table 2.** 2D test case1 (M=0.63, α=2°)

| Parameter | Roe 2nd order | IGR_Roe | SW 2nd order | IGR_SW | GAMM (1986) |
|---|---|---|---|---|---|
| CL | 0.3071 | 0.3054 | 0.3048 | 0.2921 | 0.3335 |
| CD | 0.11E-05 | 0.29E-02 | -0.95E-03 | 0.91E-02 | 0.0 |

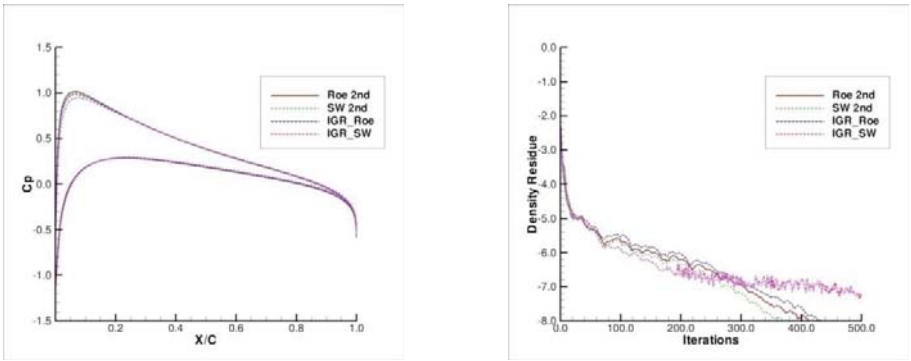


(a) (b)

**Figure 6.** Comparison between various schemes for Euler solution at M=0.63, α=2° (a) Cp plot (b) Density residue

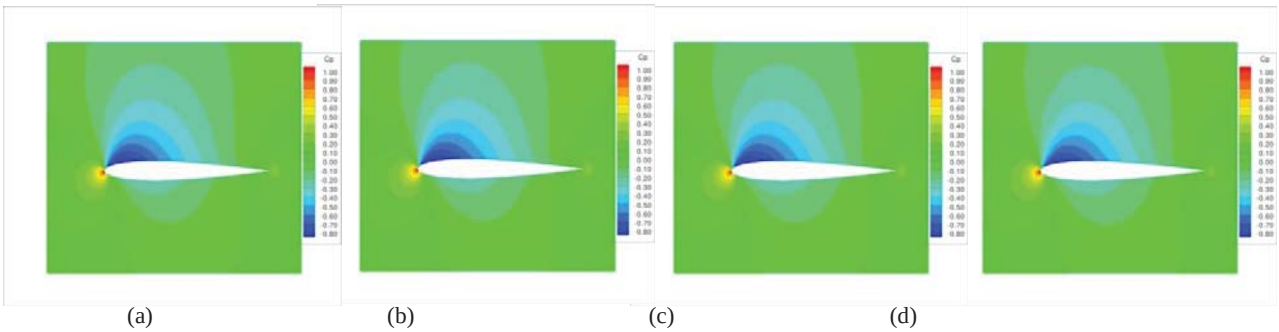

(a) (b) (c) (d)

**Figure 7.** Comparison of Cp contour for various schemes for Euler Solution at M=0.63, α=2° (a) Roe 2nd order (b) IGR_Roe (c) SW 2nd order (d) IGR_SW

*3.2.2 Case 2:* The second test case is standard AGARD test case [8] at transonic speed with M=0.85 and α=1°. In this test case, shocks wave appears on both upper and lower surfaces. Figure 8(a) shows the Cp comparison between various schemes. IGR_Roe computations compares quite well with 2nd order Roe and SW results. Figure 8(b) shows convergence plot of density residue. The Cp contour plots are given in figures 9(a)-9(d) for various schemes. Shock wave formation on lower and upper surfaces can be seen clearly in these figures. Table 3 summarizes the CL and CD comparison for this test case.

**Table 3.** 2D test case2 (M=0.85, α=1°)

| Parameter | Roe 2nd order | IGR_Roe | SW 2nd order | IGR_SW | AGARD (1985) |
|---|---|---|---|---|---|
| CL | 0.325 | 0.342 | 0.327 | 0.293 | 0.330-0.389 |
| CD | 0.0533 | 0.0564 | 0.0524 | 0.0573 | 0.0464-0.0590 |

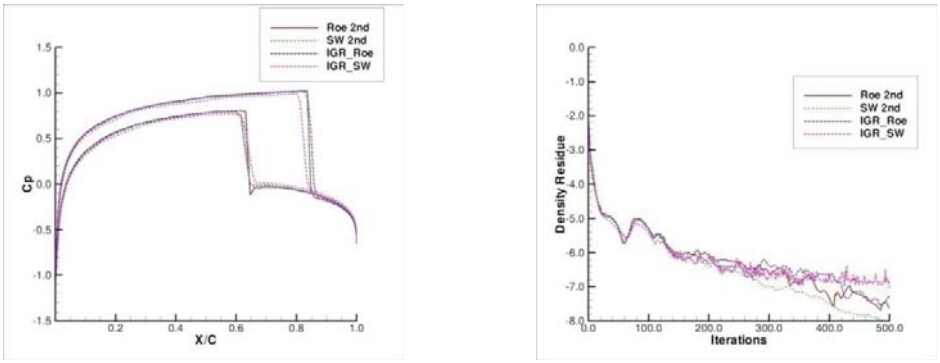


(a) (b)

**Figure 8.** Comparison between various scheme for Euler solution at M=0.85, α=1° (a) Cp plot (b) Density residue

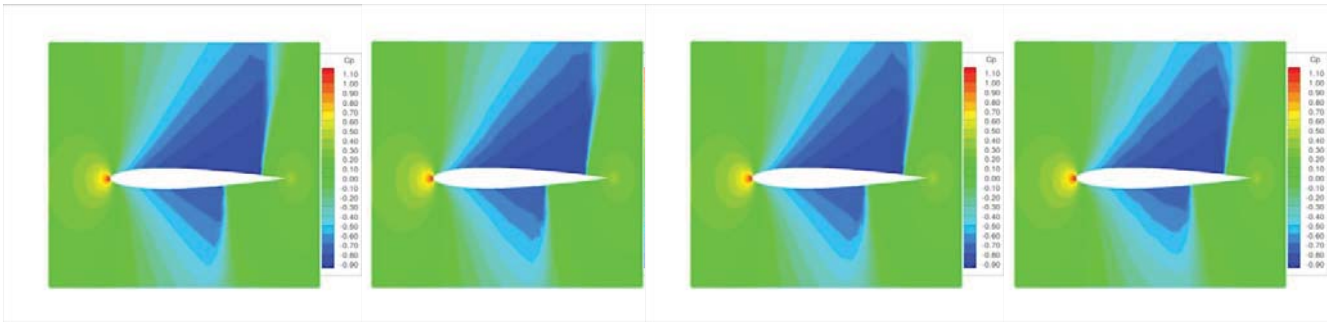

(a) (b) (c) (d)

**Figure 9.** Comparison of Cp contour for various schemes for Euler Solution at M=0.85, α=1° (a) Roe 2nd order (b) IGR_Roe (c) SW 2nd order (d) IGR_SW

*3.2.3 Case 3:* The laminar flow over NACA 0012 airfoil at M=0.5, α=3° and Reynolds number (Re) of 5000 is taken as 3rd test case. The Cp and skin friction coefficient obtained from IGR_Roe and Roe 2nd order computations are shown in Figures 10(a) and 10(b), respectively. These computations are compared with reference data available in reference [9]. The IGR_Roe and 2nd order Roe schemes are slightly under-predicting the suction peak. This is due to coarse unstructured triangular grid that we have used. However, there is good agreement between computations and reference data for skin friction coefficient. More details about pressure drag ($CD_p$), skin friction drag ($CD_f$), lift coefficient (CL) and separation location is given in

table 4.

**Table 4.** 2D test case3 (M=0.50, α=3°, Re=5000)

| | $CD_p$ | $CD_f$ | $CD_{total}$ | CL | $X_{sep}$ (% of chord) |
|---|---|---|---|---|---|
| Roe 2nd order | 0.0336 | 0.0343 | 0.0679 | 0.0521 | 46.1 |
| IGR_Roe | 0.0347 | 0.0377 | 0.0724 | 0.0404 | 50.7 |
| Venkatakrishnan(1990) | 0.0262 | 0.0321 | 0.0589 | 0.0464 | 46.4 |

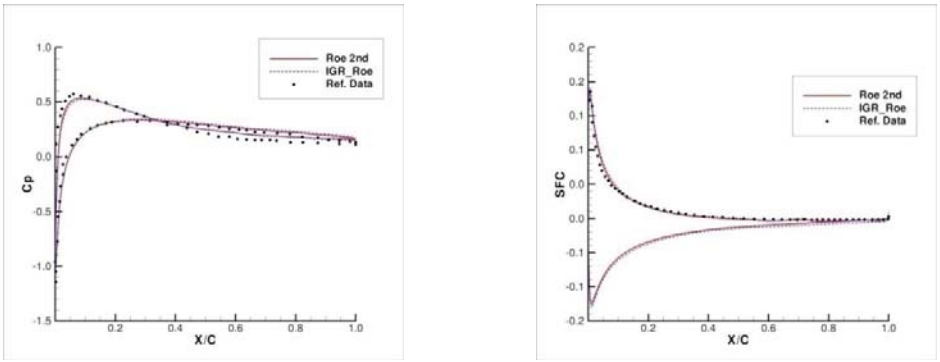


(a) (b)

**Figure 10.** Comparison between various schemes for laminar flow at M=0.50, α=3°, Re=5000 (a) Cp plot (b) Skin friction coefficient

## 4. Conclusions

The work establishes an Implicit Gradient Reconstruction procedure modifying the classical CIR scheme using the $\phi$ parameter. The accuracy of the procedure is established by solving standard test problems in 1D and 2D. As the proposed procedure offers second order accuracy without the need to store solution gradients, the memory foot print is considerably small. This feature is expected to result in significantly enhanced cache utilization for large scale 3D problems on supercomputing platforms with several thousand processor cores, enabling super-optimal utilization of such platforms. In addition, the work also opens out a framework for moderating dissipation associated with individual waves for some of the well established flux formula. The present effort is going on in further fine tuning the $\phi$ parameter to make the IGR scheme operational for a larger class of problems.

## References

[1] Ramesh V and Deshpande SM 2004 *Fluid Mechanics report*, **FM-20**, *Dept of Aerospace Engg., Indian Institute of Science, Bangalore, India.*
[2] Ramesh V and Deshpande SM 2007 *Computers and Fluids* **36** 1592
[3] Singh MK, Ramesh V and Balakrishnan N 2015 *Engineering Applications of Computational Fluid Mechanics* **9** 382
[4] Steger JL and Warming RF 1981 *Journal of Computational Physics* **40** 263
[5] [Roe PL 1981 *Journal of Computational Physics* **43** 357
[6] Sod GA 1978 Journal of Computational Physics **27** 1
[7] GAMM workshop 1986
[8] Viviand H 1985 *AGARD AR-211*
[9] Venkatakrishanan V 1990 *Computers and Fluids* **18** 191